Probing zero modes of a defect in a Kitaev quantum wire

Sheng-Wen Li (李圣文),[1,2,3] Zeng-Zhao Li (李增朝),[1] C. Y. Cai (蔡丞韻),[3,4] and C. P. Sun (孙昌璞)[1,3]

[1]*Beijing Computational Science Research Center, Beijing 100084, China*

[2]*School of Engineering and Information Technology, University of New South Wales at the Australian Defense Force Academy, Canberra, ACT 2600, Australia*

[3]*Synergetic Innovation Center of Quantum Information and Quantum Physics, University of Science and Technology of China, Hefei, Anhui 230026, China*

[4]*State Key Laboratory of Theoretical Physics, Institute of Theoretical Physics, University of Chinese Academy of Sciences, Beijing 100190, China*

(Received 10 December 2013; revised manuscript received 12 February 2014; published 9 April 2014)

The Kitaev quantum wire (KQW) model with open boundary possesses two Majorana edge modes. When the local chemical potential on a defect site is much higher than that on other sites and than the hopping energy, the electron hopping is blocked at this site. We show that the existence of such a defect on a closed KQW also gives rise to two low-energy modes, which can simulate the edge modes. The energies of the defect modes vanish to zero as the local chemical potential of the defect increase to infinity. We develop a quantum Langevin equation to study the transport of KQW for both open and closed cases. We find that when the lead is contacted with the site beside the defect, we can observe two splitted peaks around the zero-bias voltage in the differential conductance spectrum, whereas if the lead is contacted with the bulk of the quantum wire far from the the defect or the open edges, we cannot observe any zero-bias peak.

DOI: 10.1103/PhysRevB.89.134505 PACS number(s): 74.50.+r, 73.23.−b, 74.78.Na

I. INTRODUCTION

The emergent Majorana fermion in condensed matter system has attracted much attention for its novel non-Abelian statistical property and potential application in topological quantum computation [1–3]. The Kitaev quantum wire (KQW) model with open boundary possesses two localized Majorana edge modes at the two ends [4]. The realization of this quantum wire model was also reported with the help of strong spin-orbit coupling and Zeeman field in proximity to an s-wave superconductor [5–9].

To detect the existence of the Majorana fermion in the quantum wire, people can measure the differential conductance in transport experiments [10–13]. It was predicted that there is a zero-bias peak (ZBP) in the dI/dV profile in the topological phase when the quantum wire is contacted with a normal lead, and the height of the peak is $2e^2/h$ at zero temperature. Moreover, if there exists finite coupling between the Majorana fermions at the two ends, this ZBP would split into two peaks [12]. However, it was recognized that such feature of a single ZBP is not an unambiguous evidence, because similar ZBP may be also induced by different mechanisms, such as the Kondo effect [14–18].

When the local chemical potential μ_p on a defect site is much higher than that on other sites and the hopping energy, the electron hopping is blocked at this site. Thus, the existence of such a defect on a closed wire is similar to cutting off the wire at this position and generating new boundaries. Such a "cutoff" for a closed KQW also gives rise to a pair of low-energy modes (we call them the *defect modes*) [19–21]. These defect modes have many similar properties to the Majorana edge modes as follows:

(1) when the defect becomes "strong," i.e., the chemical potential μ_p of the defect becomes quite large, the energies of the defect modes approach zero;

(2) the energies of the defect modes are gapped from the bulk band of the quantum wire;

(3) the defect modes are superpositions of both electron and hole modes with equal weight, localized around the defect site.

If μ_p approaches infinity, electron hopping is fully blocked and the quantum wire can be regarded as completely cut off, thus the defect modes become Majorana edge modes. In this sense, a close quantum wire with a defect is equivalent to a homogenous open wire.

However, in practice, the strength of the defect is finite, thus there remains a small energy splitting between the two defect modes. In contrast, the energy splitting of Majorana edge modes in an open wire is practically too small to be observed even for a short chain [22]. Throughout this paper, we call both the edge and defect modes the *zero modes*.

With the above understanding, in this paper, we study the transport measurement in KQW for two kinds of configurations, i.e., a homogenous open wire and a closed wire with a defect. The detection of such zero modes induced by defect also helps test the existence of Majorana fermions [23,24]. We derive a quantum Langevin equation to describe the electrical current transport of the quantum wire contacted with two normal leads, which could give exact numerical results [22,25–28]. We obtain the differential conductance when one of the leads is contacted with different sites of the quantum wire [29]. We find that if the lead is contacted beside the defect, we can observe two splitted ZBPs in the dI/dV profile. Moreover, if the lead is contacted with other sites in the bulk of the chain far from the defect or the open edges, we cannot observe any ZBP, because the zero modes, both the edge and defect modes, are localized.

We arrange our paper as follows. In Sec. II we give a brief review of KQW. We give a demonstration of the energy spectrum and spatial distribution of the edge and defect modes. In Sec. III we derive a quantum Langevin equation for the two contacts measurement setup and obtain the steady current formula. In Sec. IV, we show the dI/dV profiles for different

measurement configurations. Finally, we draw conclusions in Sec. V. We leave some mathematical tricks and details of derivation for the appendices.

II. ZERO MODES OF KQW

In this section, we present a brief review on KQW [4], mainly in terms of fermion operators with respect to the normal modes [30]. We present a basic analysis on the spectrum of the energy modes of the quantum wire system. We show that the existence of a defect also gives rise to localized zero modes, which are similar to the Majorana edge modes under open boundary condition.

The KQW is a one-dimensional tight-binding model plus a nearest pairing term [4]. The Hamiltonian of the quantum wire can be written as

$$\hat{H}_{\rm w} = \sum_i J(\hat{d}_i^\dagger \hat{d}_{i+1} + \hat{d}_{i+1}^\dagger \hat{d}_i) - \mu \hat{d}_i^\dagger \hat{d}_i - (\Delta \hat{d}_i^\dagger \hat{d}_{i+1}^\dagger + \Delta^* \hat{d}_{i+1} \hat{d}_i). \tag{1}$$

We denote $\mathbf{d} = (\hat{d}_1, \ldots, \hat{d}_N, \hat{d}_1^\dagger, \ldots, \hat{d}_N^\dagger)^T$, where N is the total number of the sites, and then we can rewrite $\hat{H}_{\rm w}$ in a compact matrix form,

$$\hat{H}_{\rm w} = \frac{1}{2}\mathbf{d}^\dagger \cdot \mathbf{H} \cdot \mathbf{d}, \quad \mathbf{H} = \begin{bmatrix} \mathbf{h} & \mathbf{p} \\ \mathbf{p}^\dagger & -\mathbf{h} \end{bmatrix}, \tag{2}$$

where $\mathbf{h}$ and $\mathbf{p}$ are $N \times N$ matrices, and we omit a constant energy shift here. For an open wire, we have

$$\mathbf{h} = \begin{bmatrix} -\mu & J & & \\ J & -\mu & \ddots & \\ & \ddots & \ddots & J \\ & & J & -\mu \end{bmatrix}, \quad \mathbf{p} = \begin{bmatrix} 0 & -\Delta & & \\ \Delta & 0 & \ddots & \\ & \ddots & \ddots & -\Delta \\ & & \Delta & 0 \end{bmatrix}. \tag{3}$$

For the periodic boundary condition, we should add $\mathbf{h}_{1,N} = \mathbf{h}_{N,1} = J$ and $\mathbf{p}_{1,N} = -\mathbf{p}_{N,1} = -\Delta$ to the above matrices.

The eigenmodes of $\hat{H}_{\rm w}$ can be obtained by diagonalizing the matrix $\mathbf{H}$. From $\mathbf{p}^\dagger = -\mathbf{p}^*$, $\mathbf{h}^\dagger = \mathbf{h}$, we can find that $\mathbf{H}$ has the following property [31]:

Proposition. If ε is one eigenvalue of $\mathbf{H}$ with $\vec{V} = (v_1, \ldots, v_N, w_1, \ldots, w_N)^T$ as the eigenvector, then $-\varepsilon$ is also an eigenvalue, and the corresponding eigenvector is $\vec{V}' = (v_1^*, \ldots, v_N^*, w_1^*, \ldots w_N^*)^T$.

We also present a simple proof in Appendix A. This property roots from the particle-hole symmetry and guarantees that the eigenmodes of $\hat{H}_{\rm w}$ appear as particle-hole pairs,

$$\hat{\psi}_\mu = \sum_i \varphi^\mu{}_i \hat{d}_i + \phi^\mu{}_i \hat{d}_i^\dagger, \quad \hat{\psi}_\mu^\dagger = \sum_i (\phi^\mu{}_i)^* \hat{d}_i + (\varphi^\mu{}_i)^* \hat{d}_i^\dagger := \hat{\psi}'_\mu, \tag{4}$$

where $\hat{\psi}'_\mu := \hat{\psi}_\mu^\dagger$ can be regarded as the modes for holes. But keep in mind that $\{\hat{\psi}'_\mu, \hat{\psi}_\mu\} \neq 0$ thus $\hat{\psi}'_\mu$ and $\hat{\psi}_\mu$ are not independent fermion modes. Therefore we can always diagonalize the Hamiltonian into the following form:

$$\hat{H}_{\rm w} = \frac{1}{2}\mathbf{d}^\dagger \cdot \mathbf{H} \cdot \mathbf{d} = \frac{1}{2}\sum_{\mu=1}^{N} \varepsilon_\mu \hat{\psi}_\mu^\dagger \hat{\psi}_\mu - \varepsilon_\mu \hat{\psi}_\mu \hat{\psi}_\mu^\dagger. \tag{5}$$

A homogeneous open wire possesses two localized edge modes with zero energy in the topological phase area $|\mu| < 2|J|$, but a homogeneous closed wire does not have such zero modes [4]. If the local chemical potential μ_p on a defect site (site-p) is much larger than that on other sites and than the hopping energy J, the electron hopping is blocked at this site. Thus a closed wire with a defect is similar to an open wire.

We demonstrate the energy spectrum of the quantum wire for both closed and open configurations in Fig. 1. The existence of a defect in a closed wire gives rise to two defect modes in the superconducting gap separated from the bulk band. We also see that there are two high-energy modes with $\varepsilon_\mu \simeq \pm\mu_p$ as the by-product which we do not concern in this paper. Moreover, the energies of the defect modes approach to zero when μ_p tends to infinity (Fig. 2).

We also show the spatial distributions of the edge and defect modes in Figs. 3(a)–3(d) [namely, the coefficients $\varphi^\mu{}_i$ and $\phi^\mu{}_i$ in Eq. (4)]. If we regard the defect site as a new "boundary"

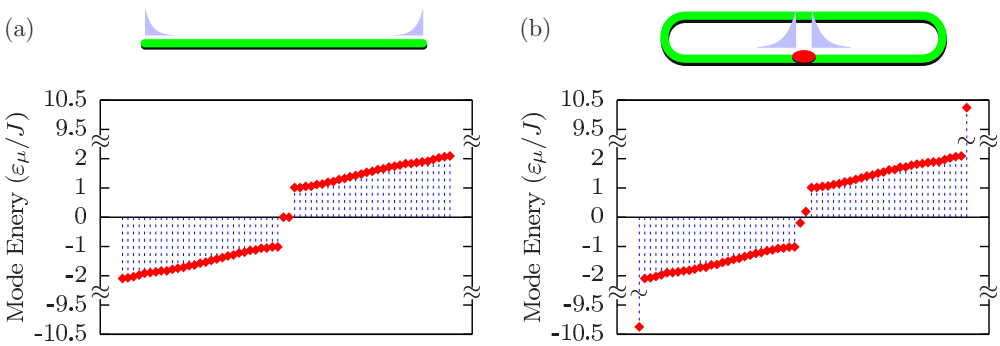

FIG. 1. (Color online) Demonstration of the energy spectrum of electrons and holes for (a) homogenous open quantum wire (b) closed quantum wire with a defect ($\mu_p = 10$). The existence of a defect gives rise to zero modes similar to open quantum wire. The chain has 30 sites, and other parameters are $\Delta = 0.5$, $\mu = 0.1$.

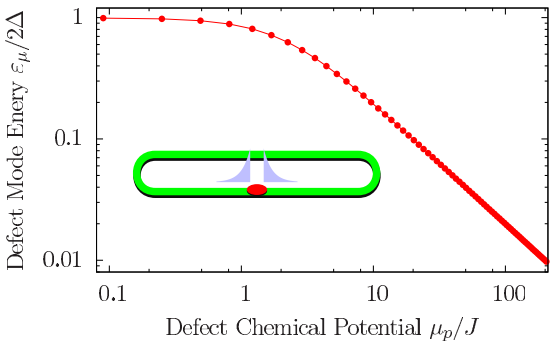

FIG. 2. (Color online) Mode energy of the defect mode in a closed wire ($N = 30$). We set $J = 1$, $\Delta = 0.6$, $\mu = 0.1$. The energy of defect mode decreases when μ_p increases.

of the quantum wire [dashed line in Figs. 3(c) and 3(d)], we see that the spatial distribution shapes of the defect modes in a closed quantum wire are almost the same with that of the Majorana edge modes in an open wire shown in Figs. 3(a) and 3(b). Therefore, in this sense, a close quantum wire with a strong defect is equivalent to a homogenous open wire.

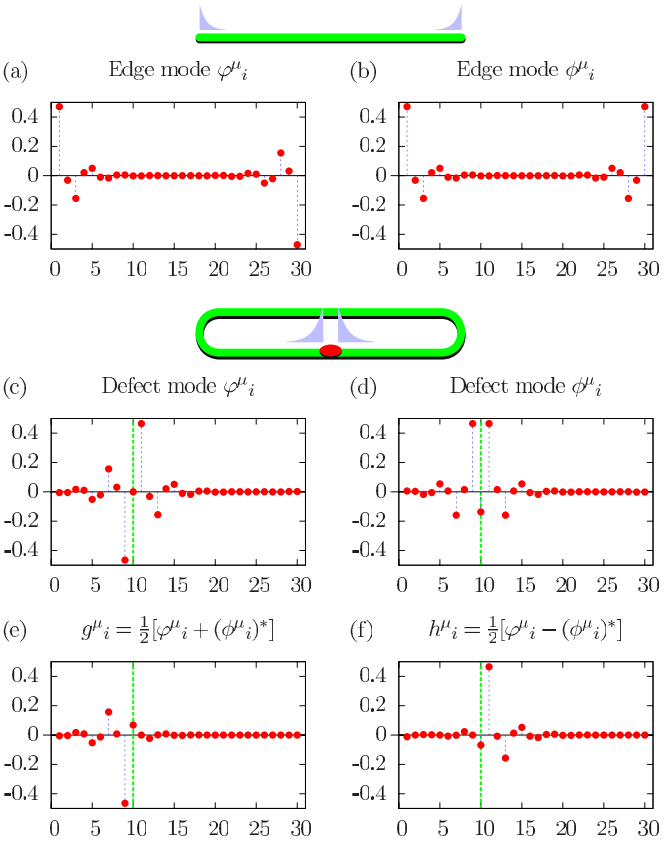

FIG. 3. (Color online) Spatial profile [$\varphi^\mu{}_i$ and $\phi^\mu{}_i$ in Eq. (4)] of [(a) and (b)] edge mode in homogenous open wire and [(c) and (d)] defect mode in closed wire. Panels (e) and (f) show the spatial profile of the Majorana operator $\hat{\gamma}_{\mu,\pm}$ [$g^\mu{}_i$ and $h^\mu{}_i$ in Eq. (6)]. The chain has 30 sites, and we set $J = 1$, $\Delta = 0.5$, $\mu = 0.1$. There is a defect with $\mu_p = 10$ at the 10-th site (represented by the green vertical line).

For these localized zero modes induced by defect, we can also represent them by the Majorana operators [4],

$$\hat{\gamma}_{\mu,+} := \hat{\psi}_\mu + \hat{\psi}^\dagger_\mu = \sum_i \left[g^\mu{}_i \hat{d}_i + \left(g^\mu{}_i\right)^* \hat{d}^\dagger_i\right],$$
$$\hat{\gamma}_{\mu,-} := -i(\hat{\psi}_\mu - \hat{\psi}^\dagger_\mu) = -i \sum_i \left[h^\mu{}_i \hat{d}_i - (h^\mu{}_i)^* \hat{d}^\dagger_i\right]. \quad (6)$$

We show the spatial distributions of $\hat{\gamma}_{\mu,\pm}$ for the defect modes in Figs. 3(e) and 3(f) [$g^\mu{}_i$ and $h^\mu{}_i$ in Eq. (6)]. They are also Majorana fermions, which are the antiparticles of themselves, i.e., $\hat{\gamma}_{\mu,\pm} = [\hat{\gamma}_{\mu,\pm}]^\dagger$. With these notations, the effective Hamiltonian for the low-energy modes can be written as

$$\hat{H}_{\text{low}} = \frac{i}{2} \sum_\mu \varepsilon_\mu \hat{\gamma}_{\mu,+} \hat{\gamma}_{\mu,-}, \quad (7)$$

where the summation includes the low-energy edge or defect modes. For an open wire with finite length, or when $|\mu_p/J|$ is not too large, ε_μ does not equal to zero exactly, and Eq. (7) is often regarded as the coupling between the Majorana fermions [4,12].

Practically, for a homogenous open wire, the energy splitting of two edge modes decays so fast with the length of the wire that we cannot observe this splitting even for a quite short chain [22]. For the defect modes, μ_p must be quite large ($|\mu_p/J| \gg 100$) to make $\varepsilon_\mu \simeq 0$ (Fig. 2). This property can be utilized to observe the splitting of the ZBP in the dI/dV spectrum.

III. QUANTUM LANGEVIN EQUATION AND STEADY CURRENT

In this section, we derive a quantum Langevin equation to study the transport behavior of KQW contacted with two electron leads and we obtain the formula for the steady current.

A. Quantum Langevin equation

We derive a quantum Langevin equation to study the transport of this quantum wire [22,25,28]. The transport measurement setup of the quantum wire is demonstrated in Fig. 4. Our derivation here is valid for both the open and closed quantum wire cases. We consider the quantum wire of N sites coupled with two normal leads via electron tunneling at site x, y ($1 \leqslant x, y \leqslant N$), respectively. The total Hamiltonian of the quantum wire and the leads can be written as

$$\mathcal{H} = \hat{H}_{\text{w}} + \hat{H}_B + \hat{H}_T, \quad (8)$$

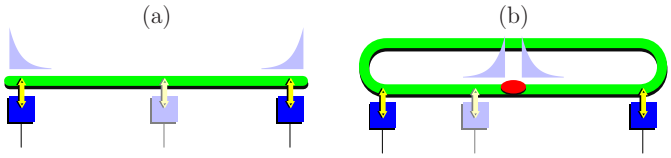

FIG. 4. (Color online) Two contacts transport measurement setup for (a) a homogenous open wire (b) a closed wire with a defect. The leads can be contacted with different sites.

where $\hat{H}_{\rm w}$ is shown in Eq. (1). $\hat{H}_B$ is the Hamiltonian for the two electron leads contacting with site x, y,

$$\hat{H}_B = \sum_{\mathbf{k}_x} \omega_{\mathbf{k}_x} \hat{c}^\dagger_{\mathbf{k}_x} \hat{c}_{\mathbf{k}_x} + \sum_{\mathbf{k}_y} \omega_{\mathbf{k}_y} \hat{c}^\dagger_{\mathbf{k}_y} \hat{c}_{\mathbf{k}_y}. \tag{9}$$

H_T describes the tunneling between the quantum wire and the leads,

$$\hat{H}_T = \hat{d}^\dagger_x \hat{\Psi}_x + \hat{\Psi}^\dagger_x \hat{d}_x + \hat{d}^\dagger_y \hat{\Psi}_y + \hat{\Psi}^\dagger_y \hat{d}_y, \tag{10}$$

where $\hat{\Psi}_x = \sum_{\mathbf{k}_x} g_{\mathbf{k}_x} \hat{c}_{\mathbf{k}_x}$.

We assume that the system evolves from $t = 0$, i.e., $\hat{d}_i(t) = \Theta(t)\hat{d}_i(t)$ and $\hat{c}_{\mathbf{k}_x}(t) = \Theta(t)\hat{c}_{\mathbf{k}_x}(t)$, and at the initial time, each lead stays at a canonical state, $\rho_x \propto \exp[-\beta_x \sum(\omega_{\mathbf{k}_x} - \mu_x)\hat{c}^\dagger_{\mathbf{k}_x}\hat{c}_{\mathbf{k}_x}]$, where μ_x is the chemical potential and $\beta_x^{-1} = T_x$ is the temperature for lead x.

We start from the Heisenberg equation [27],

$$\partial_t[\Theta(t)\hat{O}(t)] = \delta(t)\hat{O}(0) - i\Theta(t)[\hat{O}(t), \mathcal{H}], \tag{11}$$

where $\hat{O}(t)$ may be the operator $\hat{c}_{\mathbf{k}_x}(t)$ or $\hat{d}_i(t)$. The equations of motion for $\hat{c}_{\mathbf{k}_x}(t)$ and $\hat{d}_x(t)$ are

$$\begin{aligned} \partial_t \hat{c}_{\mathbf{k}_x}(t) &= \delta(t)\hat{c}_{\mathbf{k}_x}(0) - i(\omega_{\mathbf{k}_x}\hat{c}_{\mathbf{k}_x} + g^*_{\mathbf{k}_x}\hat{d}_x), \\ \partial_t \hat{d}_x(t) &= \delta(t)\hat{d}_x(0) - i[\hat{H}_{\rm w}, \hat{d}_x] - i\sum_{\mathbf{k}_x} g_{\mathbf{k}_x}\hat{c}_{\mathbf{k}_x}. \end{aligned} \tag{12}$$

We integrate the equation of $\hat{c}_{\mathbf{k}_x}(t)$ and obtain

$$\begin{aligned} \hat{c}_{\mathbf{k}_x}(t) = {}& \Theta(t)\hat{c}_{\mathbf{k}_x}(0)e^{-i\omega_{\mathbf{k}_x}t} \\ & - ig^*_{\mathbf{k}_x}\int_0^t d\tau\, e^{-i\omega_{\mathbf{k}_x}(t-\tau)}\hat{d}_x(\tau). \end{aligned} \tag{13}$$

Inserting it into the equation of $\hat{d}_x(t)$ above, we obtain a differential-integral equation,

$$\begin{aligned} \partial_t \hat{d}_x = {}& \delta(t)\hat{d}_x(0) - i[\hat{H}_{\rm w}, \hat{d}_x] \\ & - i\hat{\eta}_x(t) - \int_0^t d\tau\, D_x(t-\tau)\hat{d}_x(\tau), \end{aligned} \tag{14}$$

where

$$\begin{aligned} \hat{\eta}_x(t) &:= \Theta(t)\sum_{\mathbf{k}_x} g_{\mathbf{k}_x}\hat{c}_{\mathbf{k}_x}(0)e^{-i\omega_{\mathbf{k}_x}t}, \\ D_x(t) &:= \Theta(t)\sum_{\mathbf{k}_x} |g_{\mathbf{k}_x}|^2 e^{-i\omega_{\mathbf{k}_x}t}. \end{aligned} \tag{15}$$

Here $\hat{\eta}_x(t)$ is the random force and $D_x(t)$ is the damping kernel. These dissipation terms do not appear in the equations of $\hat{d}_i(t)$ for $i \neq x, y$.

We can write down the quantum Langevin equation for $\mathbf{d} = (\hat{d}_1, \ldots, \hat{d}_N, \hat{d}^\dagger_1, \ldots, \hat{d}^\dagger_N)^T$ in a compact matrix form,

$$\partial_t \mathbf{d} = \delta(t)\mathbf{d}(0) - i\mathbf{H}\cdot\mathbf{d} - i\boldsymbol{\eta}(t) - \int_0^t d\tau\, \mathbf{D}(t-\tau)\cdot\mathbf{d}(\tau). \tag{16}$$

Here $\mathbf{D}(t) = \mathbf{D}_x(t) + \mathbf{D}_y(t)$ is a diagonalized $2N \times 2N$ matrix, while $\boldsymbol{\eta}(t) = \boldsymbol{\eta}^x(t) + \boldsymbol{\eta}^y(t)$ is a vector of $2N$ dimension. The elements of the damping matrix $\mathbf{D}^x(t)$ are

$$[\mathbf{D}^x(t)]_{ij} = \begin{cases} D_x(t), & i = j = x, \\ D^*_x(t), & i = j = N + x, \\ 0, & \text{others.} \end{cases} \tag{17}$$

The elements of the random force vector $\boldsymbol{\eta}^x(t)$ are

$$[\boldsymbol{\eta}^x(t)]_i = \begin{cases} \hat{\eta}_x(t), & i = x, \\ -\hat{\eta}^\dagger_x(t), & i = N + x, \\ 0, & \text{others.} \end{cases} \tag{18}$$

We should also notice that the integral limit in Eq. (16) can be extended to $\pm\infty$ since we have $\mathbf{d}(t) = \Theta(t)\mathbf{d}(t)$ and $\mathbf{D}(t) = \Theta(t)\mathbf{D}(t)$. Our derivation here is valid for both the open and closed wire cases. For different quantum wire configurations, we just need to change the matrix $\mathbf{H}$ [Eq. (2)].

B. Steady current formula

Formally, the above quantum Langevin equation (16) can be solved exactly by Fourier transform,

$$\tilde{f}(\omega) = \int_{-\infty}^{\infty} dt\, \hat{f}(t)e^{i\omega t}, \quad \hat{f}(t) = \int_{-\infty}^{\infty} \frac{d\omega}{2\pi}\, \tilde{f}(\omega)e^{-i\omega t}.$$

The Fourier transform of Eq. (16) gives

$$-i\omega\tilde{\mathbf{d}}(\omega) = \mathbf{d}(0) - i\mathbf{H}\cdot\tilde{\mathbf{d}}(\omega) - i\tilde{\boldsymbol{\eta}}(\omega) - \tilde{\mathbf{D}}(\omega)\cdot\tilde{\mathbf{d}}(\omega).$$

Thus we have

$$\begin{aligned} \tilde{\mathbf{d}}(\omega) &= \tilde{\mathbf{G}}(\omega)[\mathbf{d}(0) - i\tilde{\boldsymbol{\eta}}(\omega)], \\ \tilde{\mathbf{G}}(\omega) &= i[\omega - \mathbf{H} + i\tilde{\mathbf{D}}(\omega)]^{-1}, \end{aligned} \tag{19}$$

where $\tilde{\mathbf{G}}(\omega)$ is the propagator matrix.

Here we introduce the coupling spectrum $\Gamma_x(\omega) := 2\pi\sum_{\mathbf{k}_x}|g_{\mathbf{k}_x}|^2\delta(\omega - \omega_{\mathbf{k}_x})$, and then the damping kernel $D_x(t)$ can be rewritten as

$$\begin{aligned} D_x(t) &= \Theta(t)\int_{-\infty}^{\infty}\frac{d\omega}{2\pi}\,\Gamma_x(\omega)e^{-i\omega t}, \\ \tilde{D}_x(\omega) &= \frac{1}{2}\Gamma_x(\omega) + i\mathbf{P}\int\frac{d\nu}{2\pi}\,\frac{\Gamma_x(\nu)}{\omega - \nu}. \end{aligned} \tag{20}$$

The real part of $\tilde{D}_x(\omega)$ describes the dissipation while the imaginary part is the self-energy correction. We denote $\tilde{\boldsymbol{\Gamma}}(\omega) := \tilde{\mathbf{D}} + \tilde{\mathbf{D}}^\dagger$ as the dissipation matrix, which is the real part of $2\tilde{\mathbf{D}}(\omega)$. Once the coupling spectrums of the two leads are given, in principle, we can obtain the propagator matrix $\tilde{\mathbf{G}}(\omega)$ and the dynamics of $\mathbf{d}(t)$ exactly. Here we take the spectrum to be a Lorentzian function,

$$\Gamma_x(\omega) = \Gamma_y(\omega) = \frac{\lambda\Omega_c^2}{\omega^2 + \Omega_c^2}, \tag{21}$$

where Ω_c is the cutoff frequency and λ describes the tunneling strength with the quantum wire. With this spectrum, we omit the self-energy correction.

Now we can derive the steady current when $t \to \infty$. The electrical current flowing out of the lead contacted with site x can be defined from the changing rate of the electron number

in this lead [12,23],

$$\hat{I}_x(t) = -\frac{ie}{\hbar}[\hat{d}_x^\dagger(t)\hat{\Psi}_x(t) - \hat{\Psi}_x^\dagger(t)\hat{d}_x(t)]. \tag{22}$$

In this open quantum system, the current $\overline{I}(t)$ would approach a steady state after a long time evolution. This steady current can be obtained from the Fourier transform $\tilde{I}_x(\omega)$ of $\langle \hat{I}_x(t)\rangle$ (see Appendix B),

$$\begin{aligned} \overline{I}_x(t\to\infty) &= -i\lim_{\omega\to 0}[\omega \tilde{I}(\omega)], \\ \tilde{I}_x(\omega) &= -\frac{ie}{\hbar}\int\frac{d\nu}{2\pi}\langle \tilde{d}_x^\dagger(\nu)\tilde{\Psi}_x(\nu+\omega)\rangle \\ &\quad - \langle \tilde{\Psi}_x^\dagger(\nu+\omega)\tilde{d}_x(\nu)\rangle. \end{aligned} \tag{23}$$

Recall that $\hat{\Psi}_x(t) = \sum_{\mathbf{k}_x} g_{\mathbf{k}_x}\hat{c}_{\mathbf{k}_x}(t)$, and, combining with Eqs. (13) and (15), we have

$$\tilde{\Psi}_x(\omega) = \tilde{\eta}_x(\omega) - i\tilde{D}_x(\omega)\tilde{d}_x(\omega). \tag{24}$$

With the help of the solution of $\tilde{d}_x(\omega)$ [Eq. (19)], all the expectation in $\tilde{I}_x(\omega)$ [Eq. (23)] can be expressed by the fluctuation of the random forces $\langle \tilde{\eta}_x^\dagger(\nu+\omega)\tilde{\eta}_y(\nu)\rangle$, which relates to the coupling spectrum $\Gamma_{x,y}(\omega)$ and the Fermi distribution $f_{x,y}(\omega-\mu_{x,y})$ of each lead. We obtain the formula for the steady current below (see the derivation in Appendix C),

$$\begin{aligned} \overline{I}_x(t\to\infty) = \frac{e}{\hbar}\int\frac{d\omega}{2\pi} &\tilde{\mathbf{G}}_{yx}^\dagger\Gamma_x\tilde{\mathbf{G}}_{xy}\Gamma_y(f_x - f_y) \\ &+ \tilde{\mathbf{G}}_{y+N,x}^\dagger\Gamma_y\tilde{\mathbf{G}}_{x,y+N}\Gamma_x(f_x - \overline{f}_y) \\ &+ \tilde{\mathbf{G}}_{x+N,x}^\dagger\Gamma_x\tilde{\mathbf{G}}_{x,x+N}\Gamma_x(f_x - \overline{f}_x), \end{aligned} \tag{25}$$

where we denote $f_x := f_x(\omega-\mu_x)$ and $\overline{f}_x := f_x(\mu_x-\omega) = 1 - f_x$. Here $f_x(\omega-\mu_x) := [\exp\beta_x(\omega-\mu_x)+1]^{-1}$ is the Fermi distribution.

If there is no pairing terms in the quantum wire Hamiltonian Eq. (1), $\tilde{\mathbf{G}}$ is block-diagonlized and the last two terms in Eq. (25) do not appear. In this case this formula returns to the result for a tight-binding chain [32,33]. On the other hand, the last term is similar to the current formula derived in Ref. [12], where only the Majorana subspace is considered.

We can regard $\tilde{\mathbf{G}}_{ij}(\omega)$ as the transition amplitude between different modes, and this current formula can be understood in an intuitive picture. The first term in Eq. (25) represents the transition between the local modes $\hat{d}_x$ and $\hat{d}_y$, i.e., an electron emits from lead x, and then it is received as an electron by lead y. Since there is superconducting pairing effect, the electron emitted from lead x can be also received as a hole by lead y, as represented by the second term. The last term represents the transition between the electron and hole modes both at site x, and indeed this term gives the main contribution to the ZBPs that come from the zero modes.

IV. DIFFERENTIAL CONDUCTANCE FOR KQW

Now we have obtained the steady current. We set the chemical potential of the left lead as $\mu_x = (-e)V$, while we keep $\mu_y = (-e)V_0$ as constant. At zero temperature, $f_x(\omega-\mu_x) = \Theta(\omega-\mu_x)$, thus we obtain the differential conductance as

$$\begin{aligned} \frac{dI}{dV} = &\frac{e^2}{h}[\tilde{\mathbf{G}}_{yx}^\dagger\Gamma_x\tilde{\mathbf{G}}_{xy}\Gamma_y + \tilde{\mathbf{G}}_{y+N,x}^\dagger\Gamma_y\tilde{\mathbf{G}}_{x,y+N}\Gamma_x \\ &+ 2\tilde{\mathbf{G}}_{x+N,x}^\dagger\Gamma_x\tilde{\mathbf{G}}_{x,x+N}\Gamma_x](eV). \end{aligned} \tag{26}$$

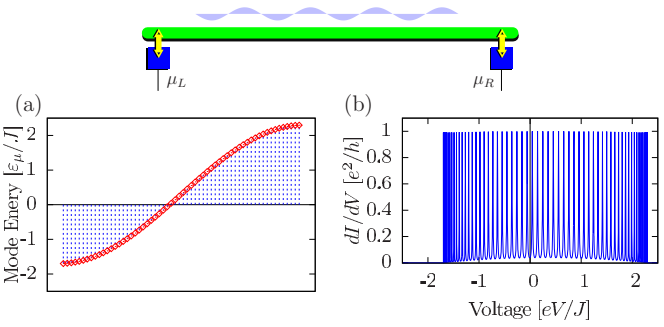

FIG. 5. (Color online) Differential conductance for a homogenous tight-binding chain ($N = 60$). We set $J = 1$, $\mu = 0.3$, $\Delta = 0$, $\lambda = 0.2$, $\Omega_c = 20$. (a) The energy spectrum. (b) The differential conductance dI/dV. The leads contact with the two ends.

The above differential conductance formula is exact. We can calculate $\tilde{\mathbf{G}}_{ij}(\omega)$ numerically to get the dI/dV spectrum. When there is no superconducting pairing term, $\Delta = 0$, the system becomes a tight-binding chain. The last two terms in Eq. (26) all vanish to zero. The energy spectrum for electron modes (no hole modes) and dI/dV profile for an open tight-binding chain is shown in Fig. 5. We see that for a homogenous tight-binding chain contacted with two leads at each end, each mode in the conducting band gives rise to a peak whose height is one conductance quantum $G_0 = e^2/h$, and the positions of the peaks correspond to the mode energies [33,34].

In Fig. 6, we show the dI/dV profile (from the left lead) in the topological phase regime that affords zero modes for different measurement configurations. We fix the position of the right lead, while the left lead can be contacted with different sites. The peaks on the two sides are contributed from the band modes, corresponding to the band structure shown in Fig. 1.

For the homogenous open wire, when the lead is contacted with the left edge [Fig. 6(a)], there is a single ZBP which is contributed from the the edge modes. The energy gap of the two edge modes can be neglected for a chain that is long enough ($N = 60$ here). If the lead is contacted with a bulk site far from the edges, we cannot observe any ZBP. Here our numerical result gives a singular point at $V = 0$. Precisely speaking, the width of this ZBP is zero, and, in practical terms, this peak is "unobservable." However, we still plot out this singular point in the picture [dashed line in Fig. 6(b)].

For the closed wire with a defect, when the lead is contacted with the nearest site beside the defect [Fig. 6(c)], we can observe two split peaks, whose positions correspond to the energies of the defect modes. Their heights are also $2e^2/h$. The distance between the two peaks depends on the strength of the defect, or, rather, the coupling between the Majorana fermions. If the lead is contacted with a bulk site far from the defect, again we cannot observe any ZBP [Fig. 6(d)].

Our results also indicate that whether a normal mode $\hat{\psi}_\mu$ [Eq. (4)] can be observed in the dI/dV spectrum depends on its overlap with the local mode $\hat{d}_x$ contacted with the lead. The

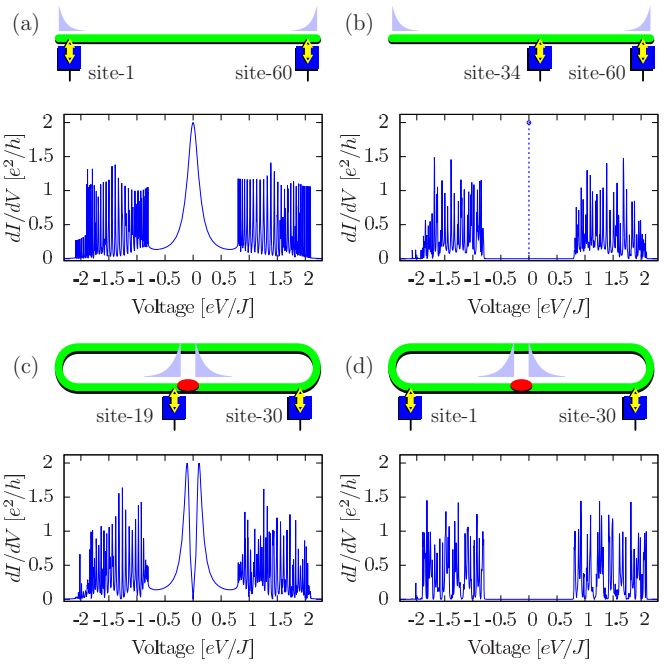

FIG. 6. (Color online) Differential conductance in topological phase regime for [(a) and (b)] a homogenous open wire and [(c) and (d)] a closed wire with a defect ($\mu_p = 15$ at site 20). We set $J = 1$, $\mu = 0.1$, $\Delta = 0.4$, $\lambda = 0.3$, $\Omega_c = 20$. The chain contains 60 sites. The position of the right lead is fixed, while the left lead is contacted with different sites.

position and strength of the defect (the chemical potential μ_p) can be controlled and tuned by applying specific gate voltage bias [19,20], and a proper defect can be "planted" as we want. Convincing evidence for Majorana fermions requires that all the features shown in Fig. 6 can be observed.

V. CONCLUSION

In this paper, we studied the transport measurement in KQW for two kinds of configurations, i.e., a homogenous open wire and a closed wire with a defect. The existence of a defect also gives rise to a pair of zero modes, which are localized superpositions of both electron and hole modes. The behavior of a defect is similar to two open edges.

We derived a quantum Langevin equation to study the two-contact transport. We obtained the formulas for the steady electrical current and differential conductance. We obtained the exact numerical result for the dI/dV spectrum when one of the leads is contacted with different site of the chain. When the lead is contacted with the edge of the open quantum wire, we can observe a single ZBP with height $2e^2/h$ contributed from the degenerated Majorana edge modes. If the lead is contacted with the site beside the defect in the closed wire, we can observe two splitted ZBPs contributed from the defect modes. The heights of the two peaks are also $2e^2/h$. When the lead is contacted with other sites in the bulk far from the defect or the open edges, no ZBP can be observed.

Base on the above results, we would suggest that a group of comparison experiments for different transport measurement configurations, as we have shown above, may be helpful to test the existence of Majorana fermions.

ACKNOWLEDGMENTS

This work is supported by National Natural Science Foundation of China under Grants No. 11121403, No. 10935010, and No. 11074261; National 973-program Grant No. 2012CB922104; and Postdoctoral Science Foundation of China Grant No. 2013M530516. S.-W.L. is grateful to the University of New South Wales at the Australian Defense Force Academy for its hospitality during his visit.

APPENDIX A: PROPERTY OF THE QUANTUM WIRE HAMILTONIAN MATRIX

Here we present the proof of the property of the Hamiltonian matrix $\mathbf{H}$ [see Eq. (2)] mentioned in Sec. II.

Proposition. If ε is one eigenvalue of $\mathbf{H}$ with $\vec{V} = (v_1, \ldots, v_N, w_1, \ldots, w_N)^T$ as the eigenvector, then $-\varepsilon$ is also an eigenvalue, and the corresponding eigenvector is $\vec{V}' = (w_1^*, \ldots, w_N^*, w_1^*, \ldots w_N^*)^T$.

Proof. The eigenequation of $\mathbf{H}\vec{V} = \varepsilon\vec{V}$ is

$$\begin{bmatrix} \mathbf{h} & \mathbf{p} \\ \mathbf{p}^\dagger & -\mathbf{h} \end{bmatrix} \begin{pmatrix} \boldsymbol{v} \\ \boldsymbol{w} \end{pmatrix} = \varepsilon \begin{pmatrix} \boldsymbol{v} \\ \boldsymbol{w} \end{pmatrix}.$$

Or we can write it as

$$\mathbf{h}_{ij} v_j + \mathbf{p}_{ij} w_j = \varepsilon v_i,$$
$$-\mathbf{p}_{ij}^* v_j - \mathbf{h}_{ij} w_j = \varepsilon w_i.$$

From the explicit form of $\mathbf{h}$ and $\mathbf{p}$ [see Eq. (3)] we should notice that $\mathbf{p}^\dagger = -\mathbf{p}^*$, $\mathbf{h}^\dagger = \mathbf{h}$. Thus the negative conjugation of the above two equations gives

$$\mathbf{h}_{ij} w_j^* + \mathbf{p}_{ij} v_j^* = -\varepsilon w_i^*,$$
$$-\mathbf{p}_{ij}^* w_j^* - \mathbf{h}_{ij} v_j^* = -\varepsilon v_i^*.$$

Or we can write it as

$$\begin{bmatrix} \mathbf{h} & \mathbf{p} \\ \mathbf{p}^\dagger & -\mathbf{h} \end{bmatrix} \begin{pmatrix} \boldsymbol{w}^* \\ \boldsymbol{v}^* \end{pmatrix} = -\varepsilon \begin{pmatrix} \boldsymbol{w}^* \\ \boldsymbol{v}^* \end{pmatrix}.$$

This is just the eigenequation $\mathbf{H}\vec{V}' = -\varepsilon\vec{V}'$. ■

APPENDIX B: GENERAL STEADY FORMULA

We want to study the long-time behavior of some dynamical observable, e.g., the electrical current $I(t \to \infty)$. Here we have a method to evaluate the long-time behavior of $I(t)$ from the poles of its Fourier transform $\tilde{I}(\omega)$.

By Fourier transform, we have

$$I(t) = \int \frac{d\omega}{2\pi} \tilde{I}(\omega) e^{-i\omega t}. \tag{B1}$$

We should notice that if $I(t)$ diverges when $t \to \infty$, indeed $\tilde{I}(\omega)$ does not exist. If $\tilde{I}(|\omega| \to \infty) \to 0$, Eq. (B1) can be integrated by the residue theorem. For $t > 0$, the contour

integral takes the lower loop, and we have

$$I(t) = -i \sum_{\substack{\text{lower}\\ \text{plane}}} \text{Res}[\tilde{I}(\omega)e^{-i\omega t}] - \frac{i}{2}\sum_{\substack{\text{real}\\ \text{axis}}} \text{Res}[\tilde{I}(\omega)e^{-i\omega t}], \tag{B2}$$

where the summations contain all the poles in the lower plane and on the real axis, respectively.

Consider the case that the pole at ω_r is simple, we have

$$\begin{aligned}\text{Res}_{\omega_r}[\tilde{I}(\omega)e^{-i\omega t}] &= \lim_{\omega\to\omega_r}[(\omega-\omega_r)\tilde{I}(\omega)e^{-i\omega t}]\\ &= e^{-i\omega_r t}\text{Res}_{\omega_r}[\tilde{I}(\omega)].\end{aligned} \tag{B3}$$

We see that all the time dependence of $I(t)$ is contained in $\exp[-i\omega_r t]$. There are three types of poles here as follows:

(1) In the lower plane, $\omega_r = \omega_0 - i\gamma$ and $\gamma > 0$. For these poles, $\exp[-i\omega_r t]$ gives rise to terms with exponential decay behavior, and they vanish when $t \to +\infty$;
(2) On the real axis, or infinitely close to it in the lower plane, $\omega_r = \omega_0 - i0^+$, but $\omega_r \neq 0$. These poles contribute to terms that keep oscillating at frequency ω_0 when $t \to +\infty$;
(3) At the origin point $\omega_r = 0$. This pole contributes a time-independent term.

Therefore, we can evaluate the long-time behavior of $I(t)$ from the poles of its Fourier transform $\tilde{I}(\omega)$. If $\tilde{I}(\omega)$ has no other poles near the real axis in the lower plane, except the simple pole $\omega_r = 0 - i\epsilon^+$, we can write down the steady state of $I(t)$ from Eq. (B2) as

$$I(t \to +\infty) = -i \lim_{\omega\to 0}[\omega\tilde{I}(\omega)]. \tag{B4}$$

For example, we consider a current that decays exponentially from $t_0 = 0$,

$$I(t) = \Theta(t)I_0(1 - e^{-i\omega_0 t - \gamma t}).$$

The Fourier transform of $I(t)$ is

$$\tilde{I}(\omega) = \frac{i}{\omega + i\epsilon^+} + \frac{i}{\omega - \omega_0 + i\gamma},$$

and we can check that Eq. (B4) holds.

APPENDIX C: STEADY CURRENT

First, we calculate the fluctuation relation of the random forces $\langle\tilde{\eta}_x^\dagger(\omega)\tilde{\eta}_y(\omega')\rangle$. The random force acting on the x-th contact site is

$$\begin{aligned}\hat{\eta}_x(t) &= \Theta(t)\sum_{\mathbf{k}_x} g_{\mathbf{k}_x} e^{-i\omega_{\mathbf{k}_x}t}\hat{c}_{\mathbf{k}_x}(0),\\ \tilde{\eta}_x(\omega) &= \sum_{\mathbf{k}_x}\frac{i g_{\mathbf{k}_x}\hat{c}_{\mathbf{k}_x}(0)}{\omega - \omega_{\mathbf{k}_x} + i\epsilon^+},\end{aligned} \tag{C1}$$

where $\tilde{\eta}_x(\omega)$ is the Fourier transform of $\hat{\eta}_x(t)$.

We have assumed that initially each reservoir stays at a canonical thermal state, which gives

$$\begin{aligned}\langle\hat{c}_{\mathbf{k}_x}^\dagger(0)\hat{c}_{\mathbf{q}_y}(0)\rangle &= \delta_{xy}f_x(\omega_{\mathbf{k}_x} - \mu_x),\\ f_x(\omega-\mu) &:= \left[\exp\frac{\omega-\mu}{kT_x} + 1\right]^{-1}.\end{aligned} \tag{C2}$$

Here $f_x(\omega - \mu)$ is the Fermi distribution, and μ is the chemical potential. Thus, we have

$$\begin{aligned}\langle\tilde{\eta}_x^\dagger(\omega)\tilde{\eta}_y(\omega')\rangle &= \sum_{\mathbf{k}_x,\mathbf{q}_y}\frac{g_{\mathbf{k}_x}^* g_{\mathbf{q}_y}\langle\hat{c}_{\mathbf{k}_x}^\dagger(0)\hat{c}_{\mathbf{q}_y}(0)\rangle}{(\omega - \omega_{\mathbf{k}_x} - i\epsilon^+)(\omega' - \omega_{\mathbf{q}_y} + i\epsilon^+)}\\ &= \int\frac{d\nu}{2\pi}\frac{\Gamma_x(\nu)f_x(\nu-\mu_x)\delta_{xy}}{(\omega - \nu - i\epsilon^+)(\omega' - \nu + i\epsilon^+)}\\ &= \frac{i\Gamma_x(\omega')f_x(\omega'-\mu_x)\delta_{xy}}{(\omega'-\omega) + 2i\epsilon^+},\\ \langle\tilde{\eta}_x(\omega)\tilde{\eta}_y^\dagger(\omega')\rangle &= \frac{i\Gamma_x(\omega')f_x(\mu_x-\omega')\delta_{xy}}{(\omega'-\omega) + 2i\epsilon^+},\end{aligned} \tag{C3}$$

where we should notice that $1 - f(\omega - \mu) = f(\mu - \omega)$. The above integrals are done by residue theorem.

From Appendix B and Eq. (23) we see that the calculation of the steady current $\bar{I}(t \to \infty)$ requires us to evaluate expectation values of the following form:

$$\langle: A(\omega)B(\omega + \delta\omega) :\rangle := -i\lim_{\delta\omega\to 0}[\delta\omega\langle A(\omega)B(\omega+\delta\omega)\rangle]. \tag{C4}$$

Here we introduce a notation $\langle: AB :\rangle$ for the simplicity of the limitation above. With this notation, from Eq. (C3) we obtain that the fluctuation of the above random forces gives

$$\begin{aligned}\langle: \tilde{\eta}_x^\dagger(\omega)\tilde{\eta}_y(\omega+\delta\omega) :\rangle &= \Gamma_x(\omega)f_x(\omega-\mu_x)\delta_{xy},\\ \langle: \tilde{\eta}_x(\omega)\tilde{\eta}_y^\dagger(\omega+\delta\omega) :\rangle &= \Gamma_x(\omega)f_x(\mu_x-\omega)\delta_{xy}.\end{aligned} \tag{C5}$$

Further, recall that

$$\begin{aligned}\tilde{\mathbf{d}}(\omega) &= \tilde{\mathbf{G}}(\omega)[\mathbf{d}(0) - i\tilde{\boldsymbol{\eta}}(\omega)],\\ \tilde{\Psi}_x(\omega) &= \tilde{\eta}_x(\omega) - i\tilde{D}_x(\omega)\tilde{d}_x(\omega),\end{aligned}$$

and then we have

$$\begin{aligned}\langle: \tilde{d}_x^\dagger\tilde{\Psi}_x :\rangle = \Big\langle: &i\sum_j\tilde{\boldsymbol{\eta}}_j^\dagger\mathbf{G}_{jx}^\dagger\tilde{\eta}_x - i\sum_{i,j}\tilde{\boldsymbol{\eta}}_j^\dagger\mathbf{G}_{jx}^\dagger D_x\mathbf{G}_{xi}\tilde{\boldsymbol{\eta}}_i\\ &+\sum_j\hat{d}_j^\dagger(0)\tilde{\mathbf{G}}_{jx}^\dagger(\tilde{\eta}_x - iD_x\tilde{d}_x)\\ &+\sum_{i,j}\tilde{\boldsymbol{\eta}}_j^\dagger\tilde{\mathbf{G}}_{jx}^\dagger D_x\tilde{\mathbf{G}}_{xi}\hat{d}_i(0) :\Big\rangle.\end{aligned}$$

The last two terms containing information from the initial state vanish to zero after long-time evolution. This can be also verified by calculating the limitation. Some straightforward calculation shows that the steady current Eq. (23) becomes

$$\begin{aligned}\bar{I}_x(t\to\infty) &= -\frac{ie}{\hbar}\int\frac{d\nu}{2\pi}\{\tilde{d}_x^\dagger\tilde{\Psi}_x - \Psi_x^\dagger d_x :\rangle\\ &= \frac{e}{\hbar}\int\frac{d\nu}{2\pi}\Big\langle: \tilde{\eta}_x^\dagger[\tilde{\mathbf{G}}^\dagger\tilde{\boldsymbol{\Gamma}}\tilde{\mathbf{G}}]_{xx}\tilde{\eta}_x\\ &\quad - \sum_i\tilde{\boldsymbol{\eta}}_i^\dagger\tilde{\mathbf{G}}_{ix}^\dagger\Gamma_x\tilde{\mathbf{G}}_{xi}\tilde{\boldsymbol{\eta}}_i :\Big\rangle.\end{aligned} \tag{C6}$$

Here we used the following relation:

$$\begin{aligned}\tilde{\mathbf{G}}+\tilde{\mathbf{G}}^{\dagger} &= \tilde{\mathbf{G}}[i(\omega-\mathbf{H}-i\tilde{\mathbf{D}}^{\dagger})-i(\omega-\mathbf{H}+i\tilde{\mathbf{D}})]\tilde{\mathbf{G}}^{\dagger}\\ &= \tilde{\mathbf{G}}\tilde{\mathbf{\Gamma}}\tilde{\mathbf{G}}^{\dagger}=\tilde{\mathbf{G}}^{\dagger}\tilde{\mathbf{\Gamma}}\tilde{\mathbf{G}},\end{aligned} \tag{C7}$$

where $\tilde{\mathbf{\Gamma}}=\tilde{\mathbf{D}}+\tilde{\mathbf{D}}^{\dagger}$ is the dissipation matrix. Finally, we can write down $\overline{I}_x$ in sum of the components as

$$\begin{aligned}\overline{I}_x(t\to\infty) =& \frac{e}{\hbar}\int\frac{d\nu}{2\pi}\tilde{\mathbf{G}}^{\dagger}_{yx}\Gamma_x\tilde{\mathbf{G}}_{xy}\Gamma_y(f_x-f_y)\\ &+\tilde{\mathbf{G}}^{\dagger}_{x+N,x}\Gamma_x\tilde{\mathbf{G}}_{x,x+N}\Gamma_x(f_x-\overline{f}_x)\\ &+\tilde{\mathbf{G}}^{\dagger}_{y+N,x}\Gamma_y\tilde{\mathbf{G}}_{x,y+N}\Gamma_x(f_x-\overline{f}_y),\end{aligned} \tag{C8}$$

where we denote $f_x := f_x(\nu-\mu_x)$ and $\overline{f}_x := f_x(\mu_x-\nu) = 1-f_x$.

[1] A. Kitaev, Ann. Phys. **321**, 2 (2006).
[2] A. Y. Kitaev, Ann. Phys. **303**, 2 (2003).
[3] C. Nayak, S. H. Simon, A. Stern, M. Freedman, and S. Das Sarma, Rev. Mod. Phys. **80**, 1083 (2008).
[4] A. Y. Kitaev, Phys. Usp. **44**, 131 (2001).
[5] V. Mourik, K. Zuo, S. M. Frolov, S. R. Plissard, E. P. A. M. Bakkers, and L. P. Kouwenhoven, Science **336**, 1003 (2012).
[6] A. Das, Y. Ronen, Y. Most, Y. Oreg, M. Heiblum, and H. Shtrikman, Nat. Phys. **8**, 887 (2012).
[7] M. T. Deng, C. L. Yu, G. Y. Huang, M. Larsson, P. Caroff, and H. Q. Xu, Nano Lett. **12**, 6414 (2012).
[8] H. O. H. Churchill, V. Fatemi, K. Grove-Rasmussen, M. T. Deng, P. Caroff, H. Q. Xu, and C. M. Marcus, Phys. Rev. B **87**, 241401 (2013).
[9] A. D. K. Finck, D. J. Van Harlingen, P. K. Mohseni, K. Jung, and X. Li, Phys. Rev. Lett. **110**, 126406 (2013).
[10] C. J. Bolech and E. Demler, Phys. Rev. Lett. **98**, 237002 (2007).
[11] K. T. Law, P. A. Lee, and T. K. Ng, Phys. Rev. Lett. **103**, 237001 (2009).
[12] K. Flensberg, Phys. Rev. B **82**, 180516 (2010).
[13] J. D. Sau, S. Tewari, R. M. Lutchyn, T. D. Stanescu, and S. Das Sarma, Phys. Rev. B **82**, 214509 (2010).
[14] S. Sasaki, S. De Franceschi, J. M. Elzerman, W. G. van der Wiel, M. Eto, S. Tarucha, and L. P. Kouwenhoven, Nature **405**, 764 (2000).
[15] E. J. H. Lee, X. Jiang, R. Aguado, G. Katsaros, C. M. Lieber, and S. De Franceschi, Phys. Rev. Lett. **109**, 186802 (2012).
[16] J. Liu, A. C. Potter, K. T. Law, and P. A. Lee, Phys. Rev. Lett. **109**, 267002 (2012).
[17] D. Rainis, L. Trifunovic, J. Klinovaja, and D. Loss, Phys. Rev. B **87**, 024515 (2013).
[18] E. J. H. Lee, X. Jiang, M. Houzet, R. Aguado, C. M. Lieber, and S. D. Franceschi, Nature Nanotech. **9**, 79 (2014).
[19] R. M. Lutchyn, T. D. Stanescu, and S. Das Sarma, Phys. Rev. Lett. **106**, 127001 (2011).
[20] J. D. Sau and E. Demler, Phys. Rev. B **88**, 205402 (2013).
[21] Y.-J. Wu, J. He, and S.-P. Kou, arXiv:1305.0114 (2013).
[22] D. Roy, C. J. Bolech, and N. Shah, Phys. Rev. B **86**, 094503 (2012).
[23] X.-J. Liu, Phys. Rev. Lett. **109**, 106404 (2012).
[24] B. M. Fregoso, A. M. Lobos, and S. Das Sarma, Phys. Rev. B **88**, 180507 (2013).
[25] A. Dhar and B. S. Shastry, Phys. Rev. B **67**, 195405 (2003).
[26] A. Dhar and D. Sen, Phys. Rev. B **73**, 085119 (2006).
[27] L.-P. Yang, C. Y. Cai, D. Z. Xu, W.-M. Zhang, and C. P. Sun, Phys. Rev. A **87**, 012110 (2013).
[28] D. Roy, C. J. Bolech, and N. Shah, arXiv:1303.7036 (2013).
[29] F. Yang, F. Qu, J. Shen, Y. Ding, J. Chen, Z. Ji, G. Liu, J. Fan, C. Yang, L. Fu, and L. Lu, Phys. Rev. B **86**, 134504 (2012).
[30] M. Leijnse and K. Flensberg, Semicond. Sci. Technol. **27**, 124003 (2012).
[31] J.-P. Blaizot and G. Ripka, *Quantum Theory of Finite Systems*, Vol. 3 (MIT Press Cambridge, MA, 1986).
[32] Y. Meir and N. S. Wingreen, Phys. Rev. Lett. **68**, 2512 (1992).
[33] S. Datta, *Quantum Transport: Atom to Transistor* (Cambridge University Press, Cambridge, UK, 2005).
[34] H. Bruus and K. Flensberg, *Many-Body Quantum Theory in Condensed Matter Physics: An Introduction* (Oxford University Press, Oxford, 2004).